Turkish Journal of Chemistry

http://journals.tubitak.gov.tr/chem/

Research Article

Turk J Chem
(2022) 46: 1723-1732

doi:10.55730/1300-0527.3475

Application of $SrFeO_3$ perovskite as electrode material for supercapacitor and investigation of Co-doping effect on the B-site

Mohammad AHANGARI[1], Elham MAHMOODI[1], Nagihan DELİBAŞ[2], Jafar MOSTAFAEI[3], Elnaz ASGHARI[3], Aligholi NIAEI[1,*]

[1]Department of Chemical and Petroleum Engineering, University of Tabriz, Tabriz, Iran
[2]Department of Physics, Faculty of Art and Science, of Sakarya University, Sakarya, Turkey
[3]Department of Physical Chemistry, Faculty of Chemistry, University of Tabriz, Tabriz, Iran

Received: 03.06.2022 • **Accepted/Published Online:** 01.09.2022 • **Final Version:** 05.10.2022

Abstract: Energy storage by supercapacitors with short charging time and high power density is one of the types of electrochemical storage systems. Perovskite oxides have been significantly investigated as promising materials for energy storage in electrochemical systems. In this study, three perovskites, $SrFeO_3$, $SrCoO_3$, and $SrCo_{0.5}Fe_{0.5}O_3$, were prepared using the sol-gel method and used as supercapacitor electrode materials. In fact, in this research, two consecutive elements (Fe, Co) from the periodic table that differ by one unit in atomic number are placed in the perovskite structure to study their electrochemical properties for use in supercapacitors. From the obtained results, it was found that Co doping with a ratio of 1/1 (Co/Fe) at B site of $SrFeO_3$ reduced the specific capacitance from 101.687 F g^{-1} to 60.912 F g^{-1} at a scan rate of 10 mV s^{-1}. Also, the specific capacitance of $SrCoO_3$ decreased from 68.639 F g^{-1} to 60.912 F g^{-1} at the same substitution rate at B site.

Key words: Supercapacitor, perovskite, oxygen vacancy, partial substitution, electrochemical performance, electrode materials

1. Introduction

With the development of industrialization, followed by an increase in environmental pollution, the production and storage of energy from renewable sources have become necessary [1–4]. In recent years, supercapacitors have been studied by many researchers due to their high energy storage performance [5–9]. Compared to batteries, these devices have high power density and good cyclic stability. They also have a higher energy density than ordinary dielectric capacitors to fill the gap between the batteries and capacitors [10–12]. Supercapacitors fall into two categories: two-layer electrical capacitors (EDLCs) and pseudocapacitors. Energy storage in EDLCs does not involve any Faraday reactions, rather, this is done through ion exchange at the electrode/electrolyte interface. An example of an electrode material used in EDLCs could be high specific surface carbon materials. Instead, pseudocapacitors store energy on the surface of conductive polymeric materials or metal oxides through Faraday reversible reactions [13–16]. Transition metal oxides are usually more stable than carbon-based materials, and have a higher energy density than conductive polymeric materials, so they are good candidates for supercapacitor electrodes [17].

Nowadays, inorganic nanoparticles have found a special place in electrochemistry applications and are widely considered by researchers. For example, the composites of $Fe@Fe_2O_3$ core-shell nanowires [18], iron minerals (magnetite, siderite, hematite, limonite and pyrite) [19] loaded on graphene respectively as a cathode in the electrofenton process to remove the drug sulfasalazine from aqueous solution. And elimination of paclitaxel as an antineoplastic drug were studied. Also, carbon nanotubes (CNTs) and double-layer CuFe nanolayer hydroxide (NLDH) [20] have been investigated for the decomposition and mineralization of the antibiotic cefazolin during the electrofenton process. Recently, these materials have been studied by researchers as electrode materials for supercapacitors.

Perovskite materials with ABO_3 structure have also been considered due to their stable structure, high concentration of oxygen vacancy and excellent capacitance [21]. Perovskite oxides ideally have the closed formula ABO_3 which have a cubic or almost cubic structure. It is possible to presence of ions in different sizes and valances in the A and B site of perovskite structure which shows the high flexibility of these compounds. In the cubic structure, each B site cation bonds

* Correspondence: ali.niaei@gmail.com

with 6 oxygen atoms to form an octagonal (BO_6) and each A site cation bonds with 12 oxygen atoms to obtain a stabilized perovskite structure [22,23]. In fact, the main controller of electrochemical properties of perovskite can be considered related to BO_6 in the structure of perovskite. In addition, the physicochemical properties of perovskites can be improved by substitution at the A and B sites with another cation with different radii and valence [24–28]. One of the properties of perovskites that lead us to study them as supercapacitor electrode is their ionic and electronic conductivity [29–35]. In 2014, Mefford et al. [36] investigated the storage of anionic charge in the LaMnO3 perovskite as a supercapacitor electrode. For the first time, they used oxygen intercalation for rapid energy storage. Zhu et al. [37] synthesized $SrCo_{0.9}Nb_{0.1}O_{3-\delta}$ for use in supercapacitor as electrode material. Their results showed that in this type of perovskite oxide, when the discharge rate increases from 0.1 to 10 A g^{-1}, the storage capacitance will be more than 92%.

In this study, the electrochemical properties of $SrCoO_3$, $SrFeO_3$, $SrFe_{0.5}Co_{0.5}O_3$ perovskites as supercapacitor electrodes were investigated to evaluate the effect of partial substitution at the B-site of $SrFeO_3$ and $SrCoO_3$ on the performance and specific capacitance of the supercapacitor electrode. As far as we know, it is may be the first time that Co and Fe elements, which differ by one unit in atomic number, are placed in the B site of the perovskite structure, and their electrochemical properties are studied as supercapacitor electrodes. The electrochemical activity of $SrFeO_3$, $SrCoO_3$ and $SrFe_{0.5}Co_{0.5}O_3$ was determined by cyclic voltametric (CV), galvanostatic charge-discharge (GCD), and electrochemical impedance spectroscopy (EIS) analyses.

2. Materials and methods

2.1. Synthesis and characterization

Raw materials include Strontium nitrate (Sr $(NO_3)_2$, assay 98.0%, Samchun, South Korea), cobalt (II) nitrate hexahydrate (Co $(NO_3)_2$.$6H_2O$, assay 97%, Merck), iron (III) nitrate nonahydrate (Fe $(NO_3)_3$.$9H_2O$, assay 99%, Merck, Germany), glycine (H_2NCH_2COOH, assay 99.0%, Samchun, South Korea). The $SrFeO_3$, $SrCoO_3$, and $SrFe_{0.5}Co_{0.5}O_3$ were synthesized by the combustion sol-gel method. The preliminary materials $Sr(NO_3)_3$, $Co(NO_3)_3.4H_2O$, and $Fe(NO_3)_3.9H_2O$ were mixed in stoichiometric ratio (to produce 1 g of $SrFeO_3$, each raw material was used: 1.105, 0, and 2.11 g, respectively. Also for $SrCoO_3$: 1.11, 1.32, and 0 g and for $SrFe_{0.5}Co_{0.5}O_3$: 1.108, 0.657, and 1.057 g of the mentioned raw materials were used, respectively.) at 60 °C in 50 mL deionized water, then glycine with a 5:1 molar ratio (glycine/perovskite; about 1.96 g of glycine is needed to produce 1 g of each of the three mentioned perovskite samples) added to the solution at 80 °C. By continued heating and stirring, the gel was formed, and by auto-combustion, a black-brown perovskite powder was obtained.

Crystalline phases were identified by X-ray diffraction (Tongda TD-3700, China) and Cu Kα radiation (λ = 1.5406 Å). Diffractograms were recorded with a step of 0.02 degree per 0.5 s for 2θ between 10 and 80. The synthesized materials were morphologically investigated by scanning electron microscopy (FE-SEM, model MIRA3-TESCAN, Czech) analysis. Further analysis of the structure was carried out by energy dispersive X-ray spectroscopy (EDX, MIRA3 FEG-SEM, Tescan, Czech Republic) analyzes and elemental mapping. The pore size distribution of samples was determined by Brunauer-Emmett-Teller (BET) through nitrogen adsorption-desorption analyzer (Micromeritics, TriStar II 3020).

2.2. Electrochemical measurement

The electrochemical evaluations were conducted using an Autolab, PGSTAT30 Potentiostat-Galvanostat. All electrochemical analysis and measurements were done in a symmetric two-electrode system. In which copper plates were used as current collectors and paper impregnated with 1 mol/L KOH (as electrolyte material) was used as separator. Cyclic voltammetry (CV) curves were obtained at various potential scan rates between −0.8 and (+1.0) V. Electrochemical impedance spectrometry (EIS) measurements were carried out at open circuit potential (OCP) in a frequency range of 100 kHz – 10 mHz. Galvanostatic charge-discharge (GCD) tests were performed in a voltage range of −0.8 to 1.0 V with different current densities. Using CV curves and GCD curves, the specific capacitance (Cs, F g^{-1}) of perovskite compounds can be obtained from Equations (1) and (2), respectively [4]:

$$C_s = \frac{1}{2\times m\times \nu\times \Delta V}\int_{V_a}^{V_c} i_{(V)}dV \quad (1)$$

$$C_s = \frac{i\times \Delta t}{m\times \Delta V}, \quad (2)$$

where (A) is the current , (g) is the mass of electrode material, (s) is the discharge time, (mV s^{-1}) is the scan rate, and (V) is the potential sweep window.

The energy density (E, Wh kg^{-1}) and power density (P, W kg^{-1}) of the supercapacitor were also obtained from the GCD curves according to Equations (3) and (4) [4, 38]:

$$E = \frac{1}{2} C_s V^2 \quad (3)$$

$$P = 3600 \times \frac{E}{\Delta t}, \mathrm{W} \quad (4)$$

where (F g^{-1}) is the specific capacitance, (V) is the potential drop.

3. Results and discussion

3.1. Crystal structure and morphology

Figure 1 shows the XRD pattern of $SrCoO_3$, $SrFeO_3$, and $SrFe_{0.5}Co_{0.5}O_3$ powders. From the obtained diffraction patterns, the peak sharpness of $SrCoO_3$, $SrFeO_3$, and $SrFe_{0.5}Co_{0.5}O_3$ occurred at angles (2θ) of 32.655°, 32.816°, and 32.803°, respectively. This showed the sharp peak of the SF shifted slightly to the left relative to the sharp peak of the $SrFe_{0.5}Co_{0.5}O_3$ while the sharp peak of the $SrCoO_3$ shifted to the right, indicating that the $SrCoO_3$ is distorted in structure of perovskite [18]. The reason for the observed shift in the XRD patterns of the synthesized samples is the difference in the elements in B site of the perovskite structure; because the oxidation states of each of the elements are different and these oxidation states directly affect the chemical bonds in the perovskite structure and cause structural differences among them. The oxygen vacancy of the perovskite structure, which is related to the oxidation states of the B site element, can be determined to some extent by the same structural differences observed from the XRD analysis of the samples. According to the obtained XRD results and comparing with the related standard XRD cards, the presence of oxygen vacancy in the structure of synthesized perovskites was confirmed. According to the obtained XRD diffraction for $SrCoO_3$ structure of this perovskite has a rhombohedral structure and its diffraction pattern according to Figure 1 is very close to $SrCoO_x$ (JCPDS card 49-0692), and after doping Fe along with Co ($SrFe_{0.5}Co_{0.5}O_3$), the structure has changed to cubic (JCPDS card 46-0335). While the structure of SrFeO is cubic, its diffraction pattern is close to $SrFeO_{2.97}$ (JCPDS card 40-0905).

The morphological structure of the synthesized perovskite compounds was obtained by SEM analysis, as shown in Figures 2a–2c. All of the synthesized perovskites have shown rough and highly porous structures that may result in an increased active surface area for the electrodes. More homogenous distribution of the pores is obvious for $SrFe_{0.5}Co_{0.5}O_3$ compared to $SrFeO_3$. Both $SrCoO_3$ and $SrFe_{0.5}Co_{0.5}O_3$ samples have also indicated small average pore sizes. These characteristics are expected to be critical factors for their supercapacitive activities. Also, analysis of nitrogen adsorption and desorption measurements was performed to obtain detailed information about the porosity nature of the synthesized samples. As shown in Figure 3 most of the pores were in the size range of 5 to 17 nm. In addition, the elemental mapping of the $SrFeO_3$ composition in Figures 2d–2g shows that the distribution of Sr, Fe and O elements on the $SrFeO_3$ surface is uniform, which confirms the success of SF synthesis. $SrFeO_3$ was also analyzed by energy dispersive X-ray (EDX). According to the EDX results as shown in Figure 2h, the molar ratios of Sr, Fe, O are 19.34, 15.78, 64.88, which is in good agreement with the theoretical values.

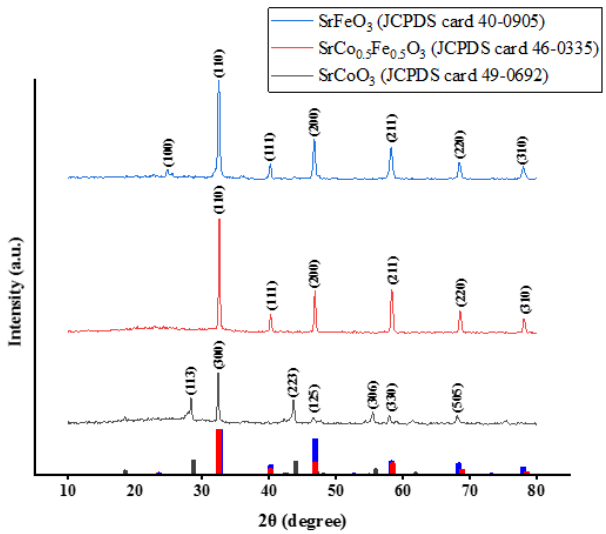

Figure 1. XRD pattern of $SrFeo_3$, $SrCo_{0.5}Fe_{0.5}O_3$, $SrCoO_3$.

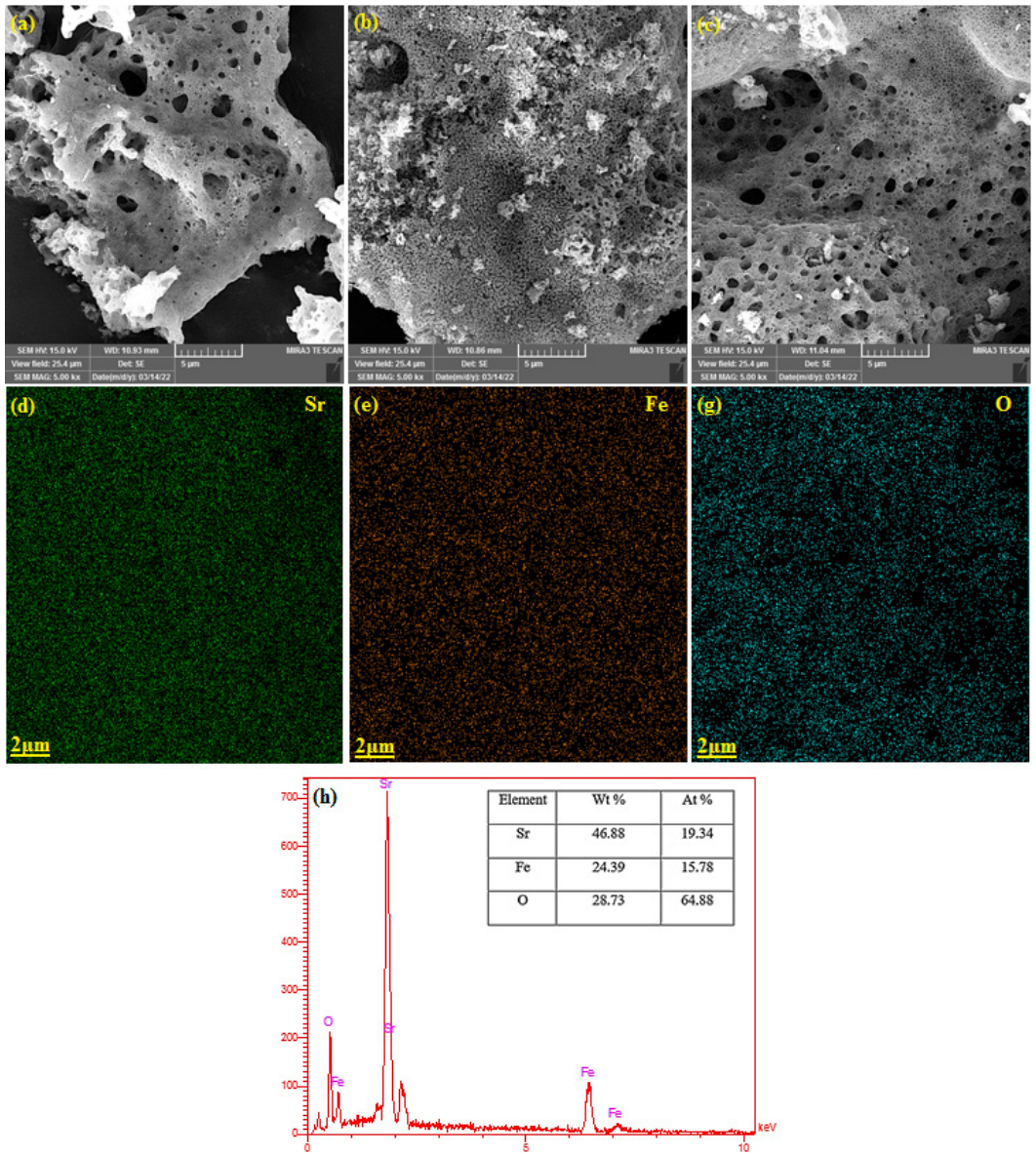

Figure 2. SEM image of (a) $SrFeO_3$, (b) $SrCoO_3$, (c) $SrCo_{0.5}Fe_{0.5}O_3$ perovskite oxide. ((d)–(g)) The elemental mapping of $SrFeO_3$. (h) EDS spectrum of sample $SrFeO_3$.

3.2. Electrochemical performance

The oxygen vacancy sites in the structure of perovskites can provide diffusion pathways for electrolyte ions. Because the compounds are synthesized in porous form, electrolyte transport is more efficient for redox reactions during the Faraday charge storage process. What is important in charge storage in this way is the mobility of oxygen vacancy space as a charge carrier. The concentration of oxygen vacancy also depends on the structure of the perovskite. In addition, the oxidation states of the B site and the ease of access to these oxidation states have a great effect on the specific capacitance (and oxygen vacancy) [39,40].

CV and GCD analysis were performed to clarify perovskite oxides' charge storage capacitance and stability, and to evaluate their specific capacitance. Figure 4 shows the CV curves of $SrCoO_3$, $SrFe_{0.5}Co_{0.5}O_3$, $SrFeO_3$ with distinct redox peaks showing typical pseudo-capacitive properties. $SrCoO_3$ and $SrFeO_3$ capacitance can be attributed to Co^{3+}/Co^{2+} and Fe^{3+}/Fe^{2+} redox reactions, respectively [41,22]. As the scan rate increases, it is observed that the area related to the CV curves increases and as a result, the specific capacitance decreases.

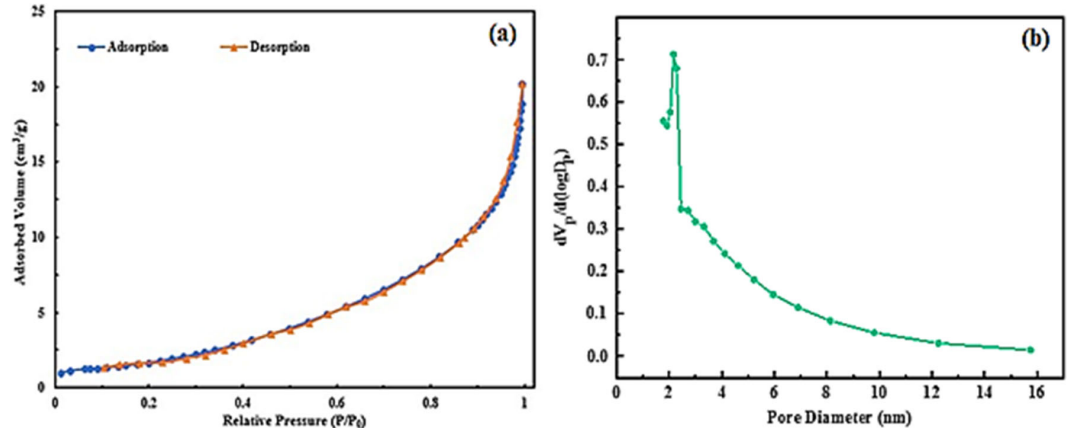

Figure 3. (a) N_2 adsorption-desorption isotherm of $SrCoO_3$, (b) Pore size distribution of $SrCoO_3$.

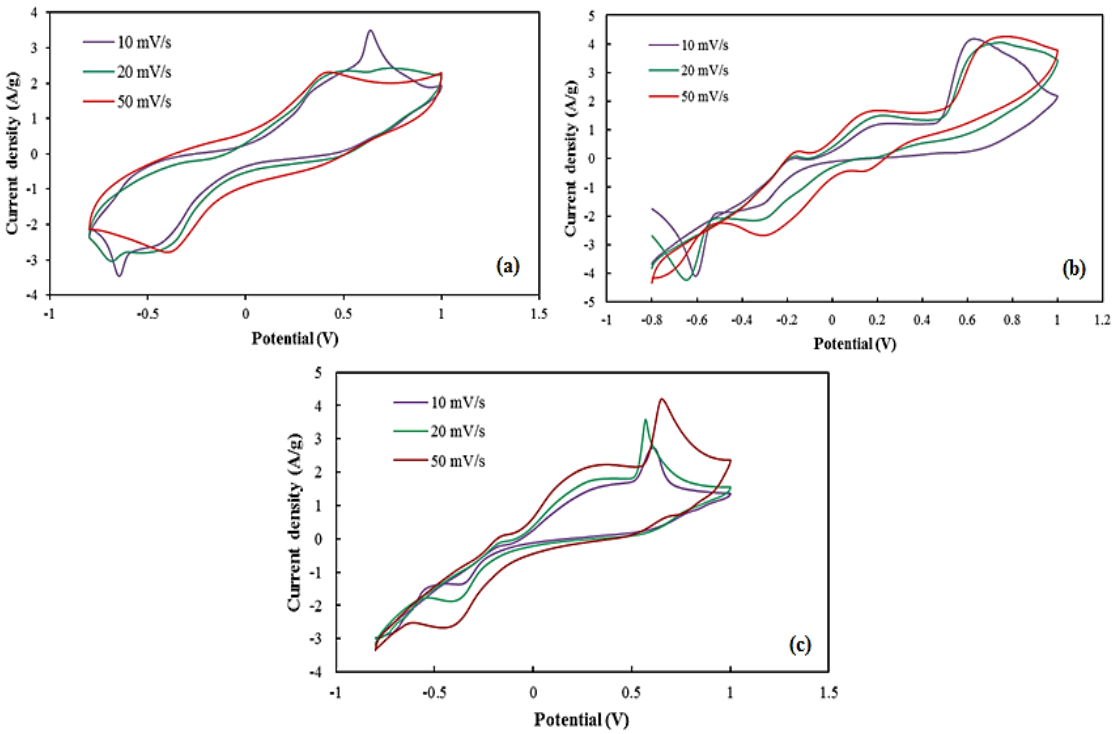

Figure 4. CV curves of (a) $SrFeO_3$, (b) $SrCoO_3$, and (c) $SrCo_{0.5}Fe_{0.5}O_3$ electrodes at different scan rates.

The decrease in specific capacitance is visible by increasing the scan rate. At lower scan rates, more electrolyte ions can react electrochemically with the active material on the electrode surface, as a result, the specific capacity increases. The specific capacitance of the synthesized perovskite compounds was calculated using the CV curve by Equation (1), the results of which are given in Table 1.

The GCD curves of the $SrCoO_3$, $SrFeO_3$ and $SrFe_{0.5}Co_{0.5}O_3$ electrodes at different current densities are shown in Figure 5. Table 2 contains information on the specific capacitance of perovskite compounds calculated from Equation 2. In addition, EIS analysis was performed in the frequency range from 100 kHz to 10 mHz. The results are shown in Figure 6. R_{ct} shows the resistance of the transfer of ions at the interface of the electrode/electrolyte materials. The straight line also shows the diffusion resistance of electrolyte ions in the pores of the electrode material [42,43]. At high frequencies, the presence of a small semicircle indicates the low charge transfer resistance (R_{ct}) at the electrode/electrolyte interface and the rapid charge propagation between the electrolyte and the perovskite electrode material.

Table 1. The specific capacitances of $SrCoO_3$, $SrFeO_3$ and $SrCo_{0.5}Fe_{0.5}O_3$ at different scan rate.

Scan rate (mV/s)	Specific capacitance (F g^{-1})		
	$SrCoO_3$	$SrFeO_3$	$SrCo_{0.5}Fe_{0.5}O_3$
10	68.639	101.687	60.912
20	26.157	51.667	43.449
50	7.646	26.108	28.99

Table 2. The specific capacitances of $SrCoO_3$, $SrFeO_3$ and $SrCo_{0.5}Fe_{0.5}O_3$ at different current densities.

Current density (A g^{-1})	Specific capacitance (F g^{-1})		
	$SrCoO_3$	$SrFeO_3$	$SrCo_{0.5}Fe_{0.5}O_3$
2	258.88	155.66	219.00
3	172.33	110.44	139.83
4	97.11	114.44	57.77

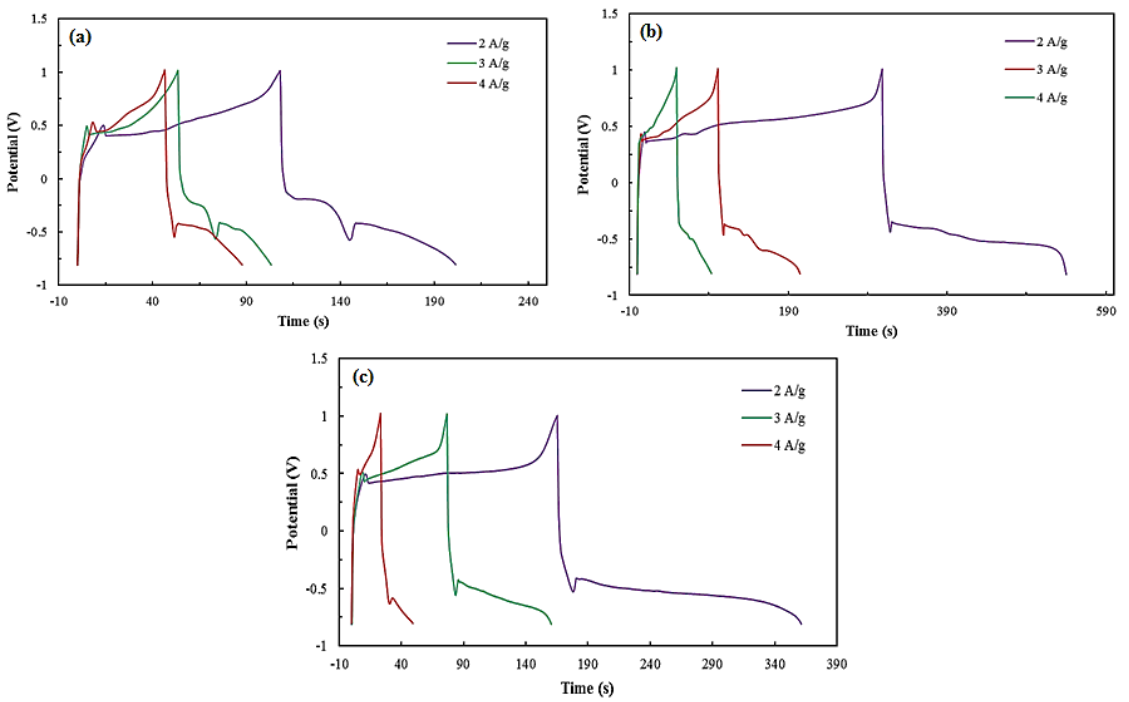

Figure 5. GCD curves of (a) $SrFeO_3$, (b) $SrCoO_3$, and (c) $SrCo_{0.5}Fe_{0.5}O_3$ electrodes at different current densities.

The results obtained for the specific capacitance of $SrFeO_3$, $SrCoO_3$ and $SrFe_{0.5}Co_{0.5}O_3$ from CV and GCD curves show that in low scanning rates and high current densities, the specific capacitances of $SrFeO_3$ are higher than those of other compounds, which could indicate the existence of the proper oxygen vacancy in the structure of this perovskite as well as the proper stability of these active points in the high current density. The partial substitution made has a negative effect on the specific capacitance of $SrFeO_3$. This means that the oxygen vacancy concentration in $SrFeO_3$ decreased after the partial substitution of Co at B site of $SrFeO_3$.

Table 3 shows the specific capacitance obtained for different compounds that have been studied as electrode material for supercapacitor. As can be seen, perovskite compounds have high specific capacitance. The main advantage of these compounds is its proper stability during redox cycles, which causes a better preservation of the specific capacitance of the perovskite supercapacitor. The compounds synthesized in this study, which have been studied as two electrodes, in other words in the symmetric cell of the supercapacitor, have specific capacitance suitable for the supercapacitor. Nevertheless, it is still possible to increase their specific capacitance with a substitution and finding the right percentage combination of A and B site elements.

4. Conclusion

In this paper, three electrode materials including $SrCoO_3$, $SrFeO_3$ and $SrCo_{0.5}Fe_{0.5}O_3$, were prepared to be used as supercapacitor electrode candidates; and the effect of partial substitution on electrochemical properties was investigated. The specific capacitance obtained for the $SrCoO_3$, $SrFeO_3$ and $SrCo_{0.5}Fe_{0.5}O_3$ samples at the scan rate of 10 mV s^{-1} was 68.639, 101.687, and 60.912 F g^{-1}, respectively, also similar to these results with a slight difference in the high current density. It was observed that accordingly $SrFeO_3$ showed higher specific capacitance at low scan rates and higher current densities than other samples. Therefore, the partial substitution of Co at the B site of $SrFeO_3$ in low scanning rates and high current densities has a negative effect on the specific capacitance and reduces it. This means that partial substitution reduces oxygen vacancy concentration as a charge carrier in the $SrFeO_3$ structure. These observations were in argument with the results of EIS, where the $SrFeO_3$ had the highest R_{ct} indicating slower charge transfer inside the electrode material, which decreases the contribution of faradaic currents in overall current density. The CV plats also confirmed this observation with a more rectangular shape of CVs for $SrFeO_3$.

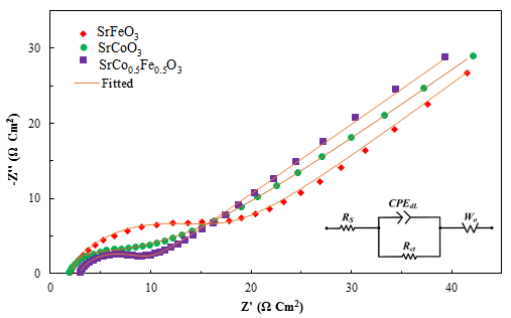

Figure 6. Electrochemical impedance spectra of $SrCoO_3$, $SrCo_{0.5}Fe_{0.5}O_3$, and $SrFeO_3$.

Table 3. The comparison different electrode materials used in supercapacitor.

Electrode materials	Specific capacitance	Electrolyte	Ref.
$CNTs/MnO_2$	1229 F g^{-1} at 1 A g^{-1}	1 mol L^{-1} Na_2SO_4	[44]
ZnO/MnO_x	556 F g^{-1} at 1 A g^{-1}	1 mol L^{-1} Na_2SO_4	[45]
CoO/NiO-Cu@CuO	2035 mF cm^{-2} at 2 mA cm^{-2}	Solid-state PVA/KOH hydrogel	[46]
CNT-Fe_3O_4	373 F g^{-1} at 10 mV s^{-1}	1 mol L^{-1} Na_2SO_4	[47]
$LaCrO_3$	1268 F g^{-1} at 2 A g^{-1}	Neutral LiCl aqueous	[48]
$SrCo_{0.9}Nb_{0.1}O_{3-\delta}$	773.6 F g^{-1} at 0.5 A g^{-1}	Aqueous KOH	[37]
$SrCoO_3$	258.88 F g^{-1} at 2 A g^{-1}	1 mol L^{-1} KOH	This work
$SrFe_{0.5}Co_{0.5}O_3$	219 F g^{-1} at 2 A g^{-1}	1 mol L^{-1} KOH	This work
$SrFeO_3$	114.44 F g^{-1} at 4 A g^{-1}	1 mol L^{-1} KOH	This work

Acknowledgment
The researchers extend their thanks and appreciation to the collaboration and support of the Department of Chemistry and Chemical and Petroleum Engineering at the University of Tabriz, the department of Physics at the University of Sakarya and the Scientific and Technological Research Council of Turkey (TUBİTAK).

References

1. Abdel Maksoud MIA, Fahim RA, Shalan AE, Abd Elkodous M, Olojede SO et al. Advanced materials and technologies for supercapacitors used in energy conversion and storage: a review. Environmental Chemistry Letters 2021; 19 (1): 375-439. https://doi.org/10.1007/s10311-020-01075-w
2. Alexander CT, Mefford JT, Saunders J, Forslund RP, Johnston KP et al. Anion-Based Pseudocapacitance of the Perovskite Library La1–xSrxBO3–δ (B = Fe, Mn, Co). ACS applied materials & interfaces 2019; 11 (5): 5084-5094. https://doi.org/10.1021/acsami.8b19592
3. Cao Y, Lin B, Sun Y, Yang H, Zhang X. Synthesis, structure and electrochemical properties of lanthanum manganese nanofibers doped with Sr and Cu. Journal of Alloys and Compounds 2015; 638: 204-213. https://doi.org/10.1016/j.jallcom.2015.03.054
4. Meng D, Gu H, Lu Q, Zhao Y, Zhu G et al. Advances and Perspectives for the Application of Perovskite Oxides in Supercapacitors. Energy & Fuels 2021; 35 (21): 17353-17371. https://doi.org/10.1021/acs.energyfuels.1c03157
5. Beidaghi M, Gogotsi Y. Capacitive energy storage in micro-scale devices: recent advances in design and fabrication of micro-supercapacitors. Energy & Environmental Science 2014; 7(3): 867-884. https://doi.org/10.1039/C3EE43526A
6. Dubal DP, Gomez-Romero P, Sankapal BR, Holze R. Nickel cobaltite as an emerging material for supercapacitors: an overview. Nano Energy 2015; 11: 377-399. https://doi.org/10.1016/j.nanoen.2014.11.013
7. Gogotsi Y, Simon P. True performance metrics in electrochemical energy storage. science 2011; 334 (6058): 917-918. https://doi.org/10.1126/science.1213003
8. Wu P, Cheng S, Yao M, Yang L, Zhu Y et al. Low-cost, self-standing NiCo2O4@ CNT/CNT multilayer electrode for flexible asymmetric solid-state supercapacitors. Advanced Functional Materials 2017; 27 (34): 1702160. https://doi.org/10.1002/adfm.201702160
9. Yang S, Zhou Y, Zhang P, Cai Z, Li Y et al. Preparation of high performance NBR/HNTs nanocomposites using an electron transferring interaction method. Applied Surface Science 2017; 425: 758-764. https://doi.org/10.1016/j.apsusc.2017.07.030
10. Chodankar NR, Dubal DP, Kwon Y, Kim DH. Direct growth of FeCo2O4 nanowire arrays on flexible stainless steel mesh for high-performance asymmetric supercapacitor. NPG Asia Materials 2017; 9 (8): e419-e419. https://doi.org/10.1038/am.2017.145
11. Hu Q, Yue B, Shao H, Yang F, Wang J et al. Facile syntheses of perovskite type LaMO3 (M = Fe, Co, Ni) nanofibers for high performance supercapacitor electrodes and lithium-ion battery anodes. Transition 2020; 1 (2): 7. https://doi.org/10.1016/j.jallcom.2020.157002
12. Lei N, Ma P, Yu B, Li S, Dai J et al. Anion-intercalated supercapacitor electrode based on perovskite-type SrB0.875Nb0.125O3 (B = Mn, Co). Chemical Engineering Journal 2021; 421: 127790. https://doi.org/10.1016/j.cej.2020.127790
13. Li W, Yang Y, Zhang G, Zhang YW. Ultrafast and directional diffusion of lithium in phosphorene for high-performance lithium-ion battery. Nano letters 2015; 15 (3): 1691-1697. https://doi.org/10.1021/nl504336h
14. Yuan C, Yang L, Hou L, Shen L, Zhang X et al. Growth of ultrathin mesoporous Co3O4 nanosheet arrays on Ni foam for high-performance electrochemical capacitors. Energy & Environmental Science 2012; 5 (7): 7883-7887. https://doi.org/10.1039/C2EE21745G
15. Zhai Y, Dou Y, Zhao D, Fulvio PF, Mayes RT et al. Carbon materials for chemical capacitive energy storage. Advanced materials 2011; 23 (42): 4828-4850. https://doi.org/ 10.1002/adma.201100984
16. Zhi M, Xiang C, Li J, Li M, Wu N. Nanostructured carbon–metal oxide composite electrodes for supercapacitors: a review. Nanoscale 2013; 5 (1): 72-88. https://doi.org/10.1039/C2NR32040A
17. Lang X, Mo H, Hu X, Tian H. Supercapacitor performance of perovskite La1– xSrxMnO3. Dalton transactions 2017; 46 (40): 13720-13730. https://doi.org/10.1039/C7DT03134C
18. Amali S, Zarei M, Ebratkhahan M, Khataee A. Preparation of Fe@ Fe2O3/3D graphene composite cathode for electrochemical removal of sulfasalazine. Chemosphere 2021; 273: 128581. https://doi.org/10.1016/j.chemosphere.2020.128581
19. Hajiahmadi M, Zarei M, Khataee A. An effective natural mineral-catalyzed heterogeneous electro-Fenton method for degradation of an antineoplastic drug: Modeling by a neural network. Chemosphere 2022; 291: 132810. https://doi.org/10.1016/j.chemosphere.2021.132810
20. Ghasemi M, Khataee A, Gholami P, Soltani RDC, Hassani A et al. In-situ electro-generation and activation of hydrogen peroxide using a CuFeNLDH-CNTs modified graphite cathode for degradation of cefazolin. Journal of environmental management 2020; 267, 110629: 13720-13730. https://doi.org/10.1016/j.jenvman.2020.110629

21. Liu Y, Dinh J, Tade MO, Shao Z. Design of perovskite oxides as anion-intercalation-type electrodes for supercapacitors: cation leaching effect. ACS Applied Materials & Interfaces 2016; 8 (36): 23774-23783. https://doi.org/10.1021/acsami.6b08634

22. Atta NF, Galal A, El-Ads EH. Perovskite nanomaterials–synthesis, characterization, and applications. Perovskite Materials–Synthesis, Characterization, Properties, and Applications; 2016; 107-151. https://doi.org/10.5772/61280

23. Assirey EAR. Perovskite synthesis, properties and their related biochemical and industrial application. Saudi Pharmaceutical Journal 2019; 27 (6): 817-829. https://doi.org/10.1016/j.jsps.2019.05.003

24. Arjun N, Pan GT, Yang TC. The exploration of Lanthanum based perovskites and their complementary electrolytes for the supercapacitor applications. Results in Physics 2017; 7: 920-926.https://doi.org/10.1016/j.rinp.2017.02.013

25. Guo Y, Shao TY, You HH, Li S, Li C et al. Polyvinylpyrrolidone-assisted solvothermal synthesis of porous LaCoO3 nanospheres as supercapacitor electrode. Int J Electrochem Sci 2017; 12: 7121-7127. https://doi.org/10.20964/2017.08.47

26. Shao T, You H, Zhai Z, Liu T, Li M et al. Hollow spherical LaNiO3 supercapacitor electrode synthesized by a facile template-free method. Materials Letters, 2017; 201: 122-124. https://doi.org/10.1016/j.matlet.2017.04.143

27. Tabari T, Singh D, Calisan A, Ebadi M, Tavakkoli H et al. Microwave assisted synthesis of La1−xCaxMnO3 (x = 0, 0.2 and 0.4): Structural and capacitance properties. Ceramics International 2017; 43 (17): 15970-15977. https://doi.org/10.1016/j.ceramint.2017.08.182

28. Wang X, Zhu W, Wang Q. Q, Zhang X. E, Zhang H. C et al. Structural and electrochemical properties of La0.85Sr0.15MnO3 powder as an electrode material for supercapacitor. Journal of Alloys and Compounds 2016; 675: 195-200. https://doi.org/10.1016/j.jallcom.2016.03.048

29. George G, Jackson SL, Luo CQ, Fang D, Luo D et al. Effect of doping on the performance of high-crystalline SrMnO3 perovskite nanofibers as a supercapacitor electrode. Ceramics International 2018; 44 (17): 21982-21992. https://doi.org/10.1016/j.ceramint.2018.08.313

30. Ma PP, Lu QL, Lei N, Liu YK, Yu B et al. Effect of A-site substitution by Ca or Sr on the structure and electrochemical performance of LaMnO3 perovskite. Electrochimica Acta 2020; 332: 135489. https://doi.org/10.1016/j.electacta.2019.135489

31. Ma PP, Zhu B, Lei N, Liu YK, Yu B et al. Effect of Sr substitution on structure and electrochemical properties of perovskite-type LaMn0.9Ni0.1O3 nanofibers. Materials Letters 2019; 252: 23-26. https://doi.org/10.1016/j.matlet.2019.05.090

32. Mo H, Nan H, Lang X, Liu S, Qiao L et al. Influence of calcium doping on performance of LaMnO3 supercapacitors. Ceramics International 2018; 44 (8): 9733-9741. https://doi.org/10.1016/j.ceramint.2018.02.205

33. Portia S, Srinivasan R, Elaiyappillai E, Johnson PM, Ramamoorthy K. Facile synthesis of Eu-doped CaTiO3 and their enhanced supercapacitive performance. Ionics 2020; 26 (7): 3543-3554. https://doi.org/10.1007/s11581-020-03494-9

34. Shafi PM, Mohapatra D, Reddy VP, Dhakal G, Kumar DR et al. Sr-and Fe-substituted LaMnO3 Perovskite: Fundamental insight and possible use in asymmetric hybrid supercapacitor. Energy Storage Materials 2022; 45: 119-129. https://doi.org/10.1016/j.ensm.2021.11.028

35. Vats AK, Kumar A, Sangwan N, Kumar A. Symmetric/asymmetric energy storage device of reduced graphene oxide assisted LaNi0.9Co0.1O3 perovskite nanomaterials. Applied Physics A 2021; 127 (12): 1-12. https://doi.org/10.1007/s00339-021-05113-4

36. Mefford JT, Hardin WG, Dai S, Johnston KP, Stevenson KJ. Anion charge storage through oxygen intercalation in LaMnO3 perovskite pseudocapacitor electrodes. Nature materials 2014; 13 (7): 726-732. https://doi.org/10.1038/nmat4000

37. Zhu L, Liu Y, Su C, Zhou W, Liu M et al. Perovskite SrCo0.9Nb0.1O3−δ as an anion-intercalated electrode material for supercapacitors with ultrahigh volumetric energy density. Angewandte Chemie 2016; 128 (33): 9728-9731. doi:10.1002/anie.201603601

38. Dong J, Lu G, Wu F, Xu C, Kang X et al. Facile synthesis of a nitrogen-doped graphene flower-like MnO2 nanocomposite and its application in supercapacitors. Applied Surface Science 2018; 427: 986-993. https://doi.org/10.1016/j.apsusc.2017.07.291

39. Nemudry A, Goldberg E. L, Aguirre M, Alario-Franco M. Á. Electrochemical topotactic oxidation of nonstoichiometric perovskites at ambient temperature. Solid state sciences 2002; 4 (5): 677-690. doi: 10.1016/S1293-2558(02)01313-4

40. Rakhi R. B, Chen W, Cha D, Alshareef H. N. Substrate dependent self-organization of mesoporous cobalt oxide nanowires with remarkable pseudocapacitance. Nano letters 2012; 12 (5): 2559-2567. https://doi.org/10.1021/nl300779a

41. Gupta A, Kushwaha V, Mondal R, Singh AN, Prakash R et al. SrFeO3− δ: a novel Fe4+↔ Fe2+ redox mediated pseudocapacitive electrode in aqueous electrolyte. Physical Chemistry Chemical Physics 2022; 24 (18): 11066-11078. https://doi.org/doi.org/10.1039/D1CP04751E

42. Gao Z, Yang W, Yan Y, Wang J, Ma J et al. Synthesis and Exfoliation of Layered α-Co(OH)2 Nanosheets and Their Electrochemical Performance for Supercapacitors. European Journal of Inorganic Chemistry 2013. 2013 (27): 4832-4838. https://doi.org/ 10.1002/ejic.201300525

43. Xu MW, Jia W, Bao SJ, Su Z, Dong B. Novel mesoporous MnO2 for high-rate electrochemical capacitive energy storage. Electrochimica Acta 2010. 55 (18): 5117-5122. https://doi.org/10.1016/j.electacta.2010.04.004

44. Jia H, Cai Y, Zheng X, Lin J, Liang H et al. Mesostructured carbon nanotube-on-MnO2 nanosheet composite for high-performance supercapacitors. ACS applied materials & interfaces 2018; 10 (45): 38963-38969. https://doi.org/10.1021/acsami.8b14109

45. Samuel E, Joshi B, Kim YI, Aldalbahi A, Rahaman M et al. ZnO/MnOx nanoflowers for high-performance supercapacitor electrodes. ACS Sustainable Chemistry & Engineering2020; 8 (9): 3697-3708. https://doi.org/10.1021/acssuschemeng.9b06796

46. Zhang A, Yue L, Jia D, Cui L, Wei D et al. Cobalt/nickel ions-assisted synthesis of laminated CuO nanospheres based on Cu(OH)2 nanorod arrays for high-performance supercapacitors. ACS applied materials & interfaces 2019; 12 (2): 2591-2600. https://doi.org/10.1021/acsami.9b20995

47. Kumar A, Sarkar D, Mukherjee S, Patil S, Sarma DD et al. Realizing an asymmetric supercapacitor employing carbon nanotubes anchored to Mn3O4 cathode and Fe3O4 anode. ACS Applied Materials & Interfaces 2018; 10 (49): 42484-42493. https://doi.org/10.1021/acsami.8b16639

48. Hussain S, Javed M. S, Ullah N, Shaheen A, Aslam N et al. Unique hierarchical mesoporous LaCrO3 perovskite oxides for highly efficient electrochemical energy storage applications. Ceramics International 2019; 45 (12): 15164-15170. https://doi.org/10.1016/j.ceramint.2019.04.258